4D Flow MRI Reveals Novel Insights Into 3D Aortic Wall Strain

T. Da Silva-Faria[1], T. Hector[1], M. S. Soulez[1], J. Leite[1], M. Moeini[1], A. Redheuil[1,2], K. Bouazizi-Verdier[1,2], U. Gencer[3], E. Mousseaux[3], G. Soulat[3], E. Bollache[1,2], N. Kachenoura[1,2]

[1]Laboratoire d'Imagerie Biomédicale (LIB), Sorbonne Université, INSERM, CNRS, Paris, France
[2]ICAN Imaging, Institute of Cardiometabolism and Nutrition (ICAN), Paris, France
[3]APHP Hôpital Européen Georges Pompidou, Université Paris Cité, PARCC, INSERM, Paris, France

Abstract

4D flow MRI provides both aortic anatomy and blood flow, but 3D regional aortic wall mechanics remain poorly characterized. We propose an automated framework to derive 3D aortic wall strain from 4D flow MRI and investigate their regional differences and relationship with aging as well as aortic volumetric distensibility in 109 healthy volunteers (45±17 years) from three sites and two vendors. Peak wall strain 3D maps were computed throughout the aorta using a pre-trained nnU-Net-derived aortic segmentation at peak systole combined with unsupervised VoxelMorph-derived deformation fields. Aortic peak wall strain was significantly associated with age (|r|≥0.34) and volumetric distensibility (|r|≥0.59) in both the ascending and descending aorta. While strain was expectedly significantly higher in the ascending than in the descending aorta, strain gradient from aortic root to celiac trunk decreased with age, reflecting well-known age-related reduced regional mismatch in aortic deformation. Although absolute wall strain differed between MRI vendors due to differences in acquisition protocols, overall physiological consistency of wall strain values was preserved suggesting reliability of our method, which could enrich readily available aortic hemodynamic assessment from a single 4D flow exam.

1. Introduction

4D flow magnetic resonance imaging (MRI) captures both aortic anatomy and blood flow velocities in the three spatial directions throughout the cardiac cycle, providing thousands of images. As such, current 4D flow analysis pipelines mostly consider segmentation of the aorta at a single peak systolic time phase to subsequently quantify functional and hemodynamic indices related to global wall stiffness [1] as well as inner blood flow patterns [2] or wall shear stress (WSS) [3]. Measures of local aortic wall elasticity as estimated from 2D MRI slices have previously demonstrated important clinical value: aortic circumferential distensibility predicts cardiovascular events and mortality in asymptomatic individuals [4], while longitudinal strain independently predicts progressive aortic dilation in patients with specific conditions like Marfan syndrome [5]. However, reliability of 2D-derived biomarkers is mitigated by through-plane motion artifacts. Regional displacement and strain mapping derived from CT [6], morphological MRI [7], or 4D ultrasound [8] has shown promising insights into aneurysm development and vascular calcification. Local aortic wall tracking from 4D flow MRI would enable simultaneous characterization of regional wall mechanics and hemodynamic biomarkers within a single examination, providing complementary information on vascular remodeling. However, to the best of our knowledge, analysis tools for strain automated quantification from 4D flow MRI are lacking, since such analyses would require time-resolved aortic segmentation which remains challenging, time-consuming and operator-dependent.

In this study, we used a deep learning-based segmentation method, integrating unsupervised motion estimation [9], to compute 3D aortic wall displacement and strain maps from 4D flow MRI acquisitions. Consistency of our method was tested in terms of expected physiological differences in derived quantitative strain metrics between the ascending (AAo) and descending (DAo) aorta, as well as their associations with age and volume change-derived aortic volumetric distensibility, in healthy volunteers across 3 sites and 2 MRI manufacturers, at 1.5 and 3 Tesla.

2. Materials and methods

2.1. Population and acquisitions

A total of 109 healthy volunteers (58 women, mean age=45±17 years) who underwent 4D flow MRI at three sites were included under local ethics committee approval, and each participant provided signed informed

consent. Sixty-two participants were scanned on 1.5T Aera (N=8) and Sola (N=54) systems (Siemens Healthineers, Vendor 1) at Sites 1 (Pitié-Salpêtrière Hospital) and 2 (IHU ICAN Research Platform); and 47 participants were scanned on a 3T Discovery MR750w GEM (GE HealthCare, Vendor 2) at Site 3 (Hôpital Européen Georges Pompidou). At all sites, 4D flow MRI was acquired in a sagittal-oblique volume covering the thoracic aorta during free breathing, with respiratory navigator and ECG gating. Population characteristics along with spatial and temporal resolutions are summarized in Table 1.

Table 1. Patients and acquisition characteristics.

	Vendor 1	Vendor 2
N (m/f)	62 (28/34)	47 (23/24)
Age (years)	41±15	49±18
Cardiac phases	20-25	50
Voxel size (mm^3)	1.8-2.5 x 1.8-2.5 x 1.9-2.5	1.1-2.4 x 1.1-2.4 x 1.0-1.1

2.2. Time-resolved segmentation

Initial aortic segmentation (M_s) at peak systole s was obtained using a previously trained nnU-Net [10]. Manual refinements were performed when necessary by an expert using 3D Slicer. Unsupervised VoxelMorph model [9] was then used to estimate dense inter-frame displacement fields $\vec{\phi}_{s\to t}$ at each remaining time phase t from 4D flow MRI anatomical images. These displacements were finally applied to M_s mesh in order to propagate aortic segmentation throughout the entire cardiac cycle, while tracking each M_s surface mesh vertex through time.

2.3. Aortic wall strain computation

Reference segmentation mesh at the first frame of the cardiac cycle (ref) comprised N surface vertices v, denoted as $V_{ref}(v)$. For each reference vertex v, a connected local surface patch $S_{ref}(v)$ was defined by considering mesh triangles with all of their 3 vertices included within a fixed 4 mm-radius neighborhood. Reference patch area $A_{ref}(v)$ was then obtained while summing areas over all mesh triangles included in $S_{ref}(v)$. The area $A_t(v)$ of the tracked local surface patch $S_t(v)$ at each cardiac phase t was computed similarly. Finally, time-resolved local wall strain was defined as the local surface area relative variation with respect to its reference value $A_{ref}(v)$, expressed for each vertex as a percentage:

$$wS_t(v) = 100 \times \left(\frac{A_t(v) - A_{ref}(v)}{A_{ref}(v)}\right),$$

providing a measure of aortic wall local deformation through time (Figure 1).

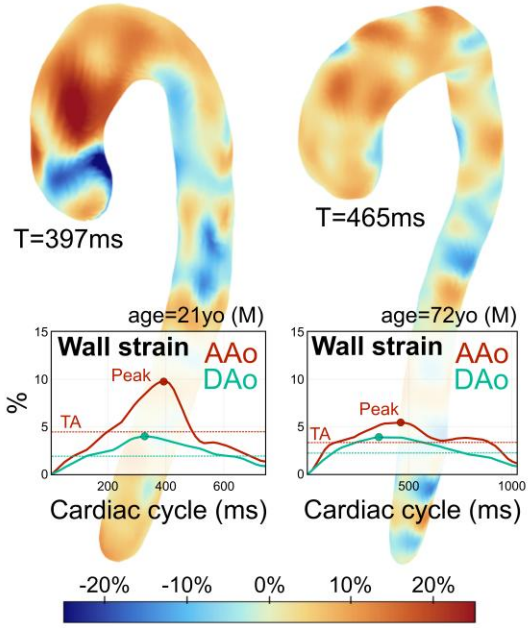

Figure 1. Examples of aortic wall strain 3D maps at peak systole and time variation strain curves in young (left) and elderly (right) individuals, along with respective peak and time-averaged (TA) values.

Wall strain was quantified separately in the AAo and DAo by spatially averaging local absolute values within each aortic segment at every time frame. Peak and time-averaged (TA) values were then extracted from the resulting wall strain time curves (Figure 1). Time-resolved segmentation masks were further used to generate 3D wall displacement maps, and corresponding peak and TA AAo and DAo displacement values were quantified.

To characterize aortic deformation changes along the aortic centerline, wall strain was also averaged in successive cross-sectional circumferences orthogonal to the aortic centerline. Peak values over the cardiac cycle were then extracted for each cross-section to build a strain profile over aortic length. Slope of such profile, which corresponds to wall strain gradient from the aortic root to the celiac trunk was estimated using a Huber regressor (Figure 2).

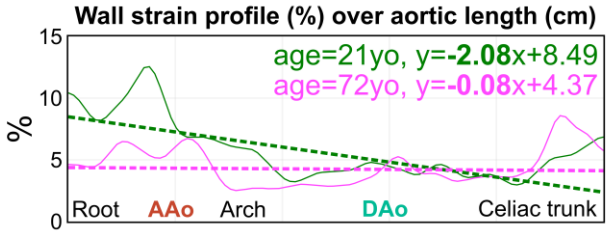

Figure 2. Examples of wall strain profile over aortic length and associated slopes in young (green) and elderly (purple) individuals.

2.4. Conventional aortic indices

AAo and DAo normalized volume change (NVC) was calculated as $NVC_{\%} = 100\frac{V_{max}-V_{min}}{V_{min}}$, where V_{max} and V_{min} denote maximum and minimum volumes over the cardiac cycle computed from segmentation masks, respectively. Aortic volumetric distensibility, which is a marker of aortic stiffness [11], was derived in 3D from NVC as follows: $D_{3D} = \frac{NVC}{PP}$, where PP_{mmHg} denotes central pulse pressure measured during MRI acquisitions. WSS was computed at each time frame and each wall point using velocity fields along with a parabolic curve-fitting approach [12]. Peak and TA WSS values were then extracted in the AAo and DAo from the resulting time-resolved WSS maps.

2.5. Statistical analyses

Variables are reported as mean ± standard deviation. Following normality check assessed using the Shapiro–Wilk test, group comparisons were performed using either Student's *t*-test or Wilcoxon rank-sum test, as appropriate. Associations of aortic AAo and DAo peak wall strain and aortic strain-length slope with age were assessed using linear regressions, and Pearson's correlation coefficient was reported (r). Similarly, association between peak wall strain and D_{3D} was assessed using linear regression.

3. Results

Table 2 summarizes aortic indices averaged over AAo and DAo segments. As expected from physiological knowledge regarding aortic wall elasticity, peak and TA wall strain, wall displacement and D_{3D} were significantly higher in the AAo compared to the DAo (p<0.005). On the other hand, peak and TA WSS values were similar across aortic segments.

Table 2. 4D flow MRI-derived aortic functional and hemodynamic indices averaged over AAo and DAo segments. TA= Time-averaged, disp.= displacement. **= p<0.005 for comparison between AAo and DAo.

	AAo	DAo
Peak wall strain (%)	6.55±1.76	3.16±1.15**
TA wall strain (%)	3.90±0.95	2.10±0.66**
Peak wall disp. (mm)	3.30±0.69	0.98±0.34**
TA wall disp. (mm)	1.83±0.45	0.60±0.19**
Volume (ml)	39.3±12.1	62.1±20.6**
D_{3D} (10^{-3} ×1/mmHg)	3.54±2.12	2.19±1.40**
Peak WSS (Pa)	0.92±0.21	1.04±0.25
TA WSS (Pa)	0.35±0.08	0.34±0.08

Figure 3 provides linear regressions of AAo and DAo peak wall strain with age and D_{3D}, stratified by MRI vendor, revealing moderate to strong correlations. Aortic strain-length slope was also moderately correlated with age (r=-0.41, p<0.005). Of note, although peak wall strain differed significantly between MRI vendors (p<0.05 in both AAo and DAo), no significant vendor effect was observed for strain-length slope (p=0.66).

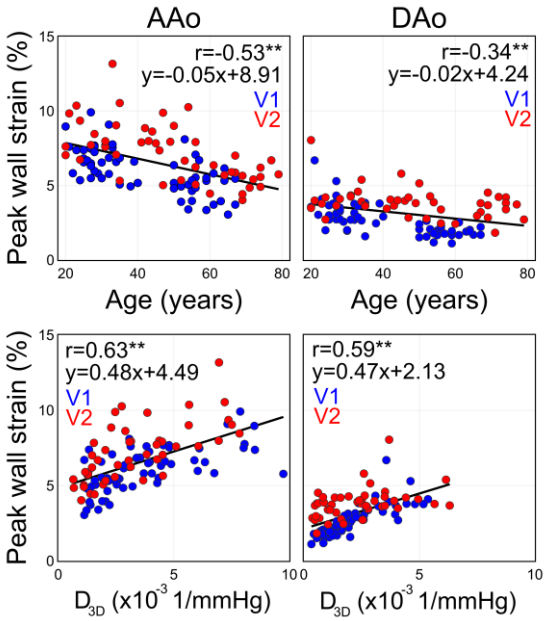

Figure 3. Associations of AAo and DAo peak wall strain with age (upper row) and D_{3D} (bottom row). V1 MRI manufacturer is highlighted in blue, and V2 in red. r= Pearson's correlation coefficient, **= p<0.005.

4. Discussion

This study demonstrates the feasibility of our original method to automatically derive regional three-dimensional aortic wall strain maps from 4D flow MRI using an unsupervised time-resolved segmentation framework. Unlike conventional global or 2D indices, the proposed approach provides comprehensive, local information on aortic wall mechanics, while enabling simultaneous assessment of hemodynamic biomarkers.

Physiological relevance of the proposed wall strain measurements observed on 109 healthy volunteers scanned at different centers through several MRI manufacturers and magnetic fields, is supported by several findings. 1) Peak and time-averaged aortic wall strain and wall displacement were consistently higher in the AAo than in the DAo, reflecting the well-documented higher compliance of the ascending aorta. Indeed, structurally, proximal aorta possesses a more functionally efficient arrangement of elastic fibers in its tunica media,

a feature that is essential for its compliance. This contrasts with distal aorta, where the elastic architecture is less organized, collagen content is higher and the vessel wall is relatively stiffer [13]. 2) Such strain gradient from aortic root to celiac trunk decreased with age, highlighting the known physiological mismatch in arterial elasticity from central arteries towards periphery early in life [14], which tends to equalize with aging as the proximal parts of the aorta progressively stiffen. 3) Peak aortic wall strain decreased significantly with age and was positively associated with volumetric distensibility, confirming its relationship with wall stiffness and sensitivity to age-related alterations in aortic elasticity.

Significant differences in peak wall strain were obtained between MRI vendors, which may be explained by differences in acquisition protocols across sites as well as imaging parameters such as temporal resolution. Indeed, lower temporal resolution is likely to reduce the ability to capture peak wall motion, particularly during systole, resulting in an underestimation of peak wall strain and displacement. Nevertheless, both vendors provided similar wall strain-length slopes, suggesting that the proposed biomarkers are robust to assess subclinical vascular remodeling despite differences in absolute values.

Although physiologically consistent, these wall strain measurements however still require further validation against independent external reference measurements. Their clinical value should also be evaluated in the context of aortic pathologies, such as aneurysms, where localized calcifications may alter wall strain spatial heterogeneity.

5. Conclusion

Consistent aortic wall strain derived from combination of 4D flow MRI and time-resolved segmentation provides complementary information to conventional hemodynamic and functional biomarkers from a single acquisition, and was able to characterize subclinical age-related vascular remodeling. Acquisition protocol standardization and investigations in patients with aortic disease are required before integrating such analysis into multicenter studies for ultimate validation.

Acknowledgements

We deeply acknowledge MRI technical staff (A Sidibé and C Ty). Study was funded in part by internal Sorbonne University grant, ANR-10-IAHU-05 and ANR-24-CE19-3961-01.

References

[1] L-A Nguyen et al, "Aortic Stiffness Measured from Either 2D/4D Flow and Cine MRI or Applanation Tonometry in Coronary Artery Disease: A Case–Control Study", *J Clin Med*, vol. 12, p. 36-43, 2023.

[2] K. Bouaou et al, "4D flow MRI aortic cross-sectional pressure changes and their associations with flow patterns in health and aneurysm", *J Cardiovasc Magn Reson*. Vol. 26, p. 101030, 2024.

[3] P. van Ooij et al, "Reproducibility and interobserver variability of systolic blood flow velocity and 3D wall shear stress derived from 4D flow MRI in the healthy aorta", *J Magn Reson Imaging*, vol. 43, p. 236–248, 2016.

[4] A. Redheuil et al., "Proximal aortic distensibility is an independent predictor of all-cause mortality and incident CV events: the MESA study", *J Am Coll Cardiol*, vol. 64, no. 24, p. 2619–2629, 2014.

[5] A. Guala et al., "Proximal aorta longitudinal strain predicts aortic root dilation rate and aortic events in Marfan syndrome", *Eur Heart J*, vol. 40, no. 25, p. 2047–2055, 2019.

[6] A. Mileto et al, "Regional Mapping of Aortic Wall Stress by Using Deformable, Motion-coherent Modeling based on Electrocardiography-gated Multidetector CT Angiography: Feasibility Study," *Radiology*, vol. 280, no. 1, p. 230–236, 2016.

[7] R. Merton et al, "Assessing aortic motion with automated 3D cine balanced steady state free precession cardiovascular magnetic resonance segmentation", *J Cardiovasc Magn Reson*, vol. 26, p. 101089, 2024.

[8] A. Hegner et al, "Using averaged models from 4D ultrasound strain imaging allows to significantly differentiate local wall strains in calcified regions of abdominal aortic aneurysms," *Biomech Model Mechanobiol*, vol. 22, no. 5, p. 1709–1727, 2023.

[9] G. Balakrishnan et al, "VoxelMorph: A Learning Framework for Deformable Medical Image Registration", *IEEE Transactions on Medical Imaging*, vol. 38, no. 8, p. 1788–1800, 2019

[10] F. Isensee et al, "nnU-Net: A self-configuring method for deep learning-based biomedical image segmentation", *Nature Methods*, vol. 18, no. 2, p. 203–211, 2021

[11] A. Pouch et al, "Dynamic Volumetric Assessment of the Aortic Root: The Influence of Bicuspid Aortic Valve Competence." *The Annals of Thoracic Surgery*, vol. 112, no. 4, p. 1317–1324, 2021.

[12] W. V. Potters et al, "Volumetric arterial wall shear stress calculation based on cine phase contrast MRI", *Journal of Magn Reson Imaging*, vol. 41, no. 2, p. 505–516, 2015.

[13] J. Concannon et al, "Quantification of the regional bioarchitecture in the human aorta", *J Anat*, vol 236, p.142-155, 2020.

[14] H Van Meurs-VanWoezik et al, "Comparison of the growth of the tunica media of the ascending aorta, aortic isthmus and descending aorta in infants and children", *J Anat*, vol 136, no.2, p. 273–281, 1983

Address for correspondence:

Tom Da Silva-Faria
15 rue de l'école de médecine, 75006, Paris, France
tom.da_silva-faria@sorbonne-universite.fr
emilie.bollache@inserm.fr
nadjia.kachenoura@inserm.fr